Available online at www.sciencedirect.com
SCIENCE DIRECT®
Journal of Solid State Chemistry 177 (2004) 1781–1788
JOURNAL OF SOLID STATE CHEMISTRY
http://elsevier.com/locate/jssc

# XAS investigation of tantalum and niobium in nanostructured $TiO_2$ anatase

Michele Sacerdoti,[a,*] Maria Chiara Dalconi,[a] Maria Cristina Carotta,[b] Barbara Cavicchi,[b] Matteo Ferroni,[b] Stefano Colonna,[c] and Maria Luisa Di Vona[d]

[a] *Dipartimento di Scienze della Terra, Università di Ferrara, Corso Ercole I d'Este, 44100 Ferrara, Italy*
[b] *Dipartimento di Fisica and INFM, Università di Ferrara, Via Paradiso, 12-44100 Ferrara, Italy*
[c] *CNR Istituto di Struttura della Materia Via Fosso del Cavaliere, 100 I-00133 Roma, Italy*
[d] *Dipartimento di Scienze e Tecnologie Chimiche, Università di Roma Tor Vergata, Via della Ricerca Scientifica, I-00133 Roma, Italy*

Received 14 July 2003; received in revised form 20 November 2003; accepted 14 December 2003

**Abstract**

Sol–gel routes were used to prepare Ta 10 at% and Nb 5 at% and 10 at% doped titania nanosized powders. When fired between 410°C and 850°C the doped titania powders are in the anatase phase; further heating up to 1050°C is required to obtain the rutile phase. The presence of dopant atoms delays the rate of transformation as compared with pure titania powders. Doping also affects the rate of grain growth and increases the conductance response to gas. To better understand the role played by dopant atoms in inhibiting both phase transformation to rutile and grain growth, X-ray Absorption Spectroscopy measurements were performed at the $L_{III}$–$L_I$ absorption edges of Ta and Nb $K$ absorption edge. Analysis was restricted to the anatase phase because the transformation to rutile phase, obtained by firing at 1050°C, is accompanied by the formation of undesired Ta and Nb oxides ($Ta_2O_5$ and $Nb_2TiO_7$, respectively). Extended X-ray Absorption Fine Structure and X-ray Absorption Near-Edge Spectroscopy analysis results indicate that in nanostructured anatase both tantalum and niobium atoms substitute Ti cations with +5 valence state.


*Keywords:* Titania; Nanosized powders; XAS; Tantalum; Niobium

## 1. Introduction

Titania films are of great interest for their optical, electrical, electrochromic as well as gas sensing properties [1]. The production of nanosized titania layers is currently the objective of research because the increased fraction of atoms located at the surface or at the grain boundaries modifies the properties of titania. Recently, thin and thick films of nanostructured titania have successfully been obtained, and some applications have greatly benefited from a nanostructured phase for $TiO_2$ [2,3].

Among the preparation procedures used, sol–gel preparation fulfils the requirements for production of nanostructured $TiO_2$. The preparation of titania powders (either pure or doped with Nb or Ta) by sol–gel technique and their characterization have previously been described, together with the evolution of the transformation from anatase to rutile [4]. From this previous investigation, it emerged that grain coalescence and the temperature of phase transition from anatase to rutile were greatly affected by the presence of dopants in the titania particles. As can be seen in Fig. 1 (reported from Ref. [4]), the temperature of the anatase–rutile phase transition is shifted to a higher temperature (1050°C) for the doped titania powders with respect to the pure titania powder. The main issue concerning the production of $TiO_2$ is the stabilization of the microstructure. In fact, thermal treatment within the 500–1000°C range activates grain growth which can be assisted by the anatase-to-rutile phase transition, resulting in exaggerated coarsening.

In anatase and rutile the titanium is coordinated to six oxygen atoms arranged in lengthened octahedral form or tetragonal dipyramids. Anatase can be conceived as an arrangement of parallel octahedra, while in the case

*Corresponding author. Fax: +39-0532-21-01-61.
*E-mail address:* m83@unife.it (M. Sacerdoti).

0022-4596/$ - see front matter © 2004 Elsevier Inc. All rights reserved.
doi:10.1016/j.jssc.2003.12.015

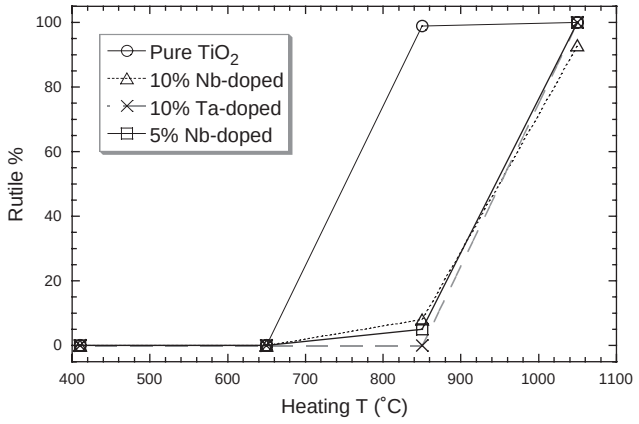


Fig. 1. Percentage of the rutile phase present in pure titania and doped titania powders as a function of the firing temperature. The rutile phase percentage has been estimated by Rietvled quantitative phase analysis (QPA) on XRD data (see Ref. [4]).

of rutile some octahedra are rotated by 90°. Therefore, conversion from anatase to rutile can be regarded in terms of reconstructive polymorphism with symmetry change from $I4_1/amd$ to $P4_2/mnm$ space group [5]. As a consequence, the high ionic mobility which occurring during phase transition results in increased densification and coarsening of the $TiO_2$ nanostructure [6].

Dopant addition in a fine-grained structure can affect the rate of grain growth and the density of rutile nucleation sites via two basic mechanisms: (i) segregation at the grain boundary, reducing the driving force for coarsening; (ii) occupation of lattice sites in such a way that it hinders ionic mobility within the particles. In this paper, we investigated the absorption edges of Nb and Ta in titania powders by X-ray absorption spectroscopy (XAS) with the aim of determining if the dopant atoms are: (i) dispersed in crystallographic sites of the anatase strucuture; (ii) segregated as a second metallic or oxide phase at grain boundaries; (iii) dispersed on the surface of the titania micrograins.

Previous X-ray absorption studies on the (Ti, Nb)$O_2$ solid solution are reported in literature [7,8]. In these studies the authors analyse the X-ray absorption *K*-edge spectra of titanium in (Ti, Nb)$O_2$ rutile solid solution or (Ti, Nb)$O_2$ amorphous thin films. There are no indications regarding the behavior of Nb dopant atoms in the anatase phase and their effect on the transformation to rutile phase.

## 2. Experimental

The titania powders doped with Nb and Ta were prepared by sol–gel technique dissolving titanium tetraisopropoxide [$Ti(OiPr)_4$] and tantalum or niobium pentaethoxide [$Ta(OEt)_5$, $Nb(OEt)_5$] in absolute ethanol under $N_2$ and added drop by drop to a solution of ethanol/water. The suspension obtained was filtered and the precipitate dried in air at 110°C for 15 h. Details are given in Refs. [4,9]. The sol–gel method was particularly suitable for homogeneous doping and control of evolution in the phase and grain size. This method allows one to achieve nanometric-sized particles with narrow grain-size distribution, and to promote nucleation of $TiO_2$ in the presence of the dopant element. Nb and Ta were added in 10% atomic ratio to Ti. Loading with 5% Nb was also used. Calcination at 410°C in air completed the synthesis, and eliminated the residual organic solvent from the powder. The obtained powders were fired in air at temperatures ranging from 650°C to 1050°C for 1 h. The powder specimens were examined by X-ray diffraction (XRD) to ensure that the single-phase anatase or rutile was obtained. XRD data were also collected for the pure titania powders calcined at 410°C (Ti410) and fired at 650°C (Ti650).

The diffraction data were recorded using a Philips PW 1820/00 vertical goniometer equipped with a graphite monochromator on the diffracted beam and with a proportional detector (PW 1711/10), operating with a Cu anode, sealed X-ray tube. A divergence slit of 0.5° and a receiving slit of 0.1 mm were used. The XRD patterns were collected in the 10°–140° $2\theta$ range with 0.02° step size, integrating 10 s per step. The recorded patterns were analyzed with the Rietveld method using the DBWS software package [10]. After synthesis and calcination at 410°C, the doped powders resulted in $TiO_2$ anatase with about 1–2% of brookite, and complete conversion into rutile was recorded after treatment at 1050°C. Unfortunately, the Ta- and Nb-doped samples fired at 1050°C contained small quantities of undesired $Ta_2O_5$ and $Nb_2TiO_7$, respectively, so they were not used in the analysis. From now on, only the doped samples with anatase structure will be discussed.

The complete set of 10% Ta-doped samples fired at 410°C, 650°C and 850°C was measured (sample names: Ta410, Ta650 and Ta850). In order to check the effect of different dopant loadings, the 5% and 10% Nb-doped samples fired at 410°C were measured (sample names: Nb5 and Nb10). The powders were mixed with boron nitride and pressed into pellets for XAS measurement; the amount of powder in the pellets was determined in order to achieve a unitary absorption edge jump. Commercially available $Ta_2O_5$, $KTaO_3$, $NaNbO_3$, $Nb_2O_5$, $NbO_2$ and NbO, as well as Ta and Nb foils, were also used as reference materials. XAS data were collected at the GILDA beam line (BM08) of the European Synchrotron Radiation Facility (Grenoble, France). A dynamically sagittally focussing monochromator [11], equipped with two Si(311) crystals, was used. Harmonics were eliminated by detuning the monochromator crystals. All measurements were performed at 77 K in order to reduce the thermal damping of the

signal. The Ta $L_{III}$-edge (energy 9881 eV) Extended X-ray Absorption Fine Structure (EXAFS) spectra and the Ta $L_I$-edge (energy 11682 eV) X-ray Absorption Near-Edge Spectroscopy (XANES) spectra were collected in the transmission mode for the Ta410, Ta650, Ta850 samples and for standard compounds $KTaO_3$ and $Ta_2O_5$. Energy calibration was regularly checked by use of a tantalum foil. The Nb *K*-edge (energy 18986 eV) EXAFS and XANES spectra were collected in the transmission mode for the Nb5 and Nb10 samples and for standard compounds NbO, $NbO_2$, $NaNbO_3$ and $Nb_2O_5$. The energy steps in the EXAFS region of the XAS spectra were chosen in order to obtain a step in the *k* scale smaller than 0.04 $Å^{-1}$. The energy step in the XANES region was 0.5 eV for the Ta $L_{III}$ and $L_I$ edges, and 1 eV for the Nb *K*-edge.

The XANES spectra were normalized in absorbance by fitting the spectral region before the pre-edge using a Victoreen function, and subtracting this as background absorption. The average absorption coefficient of the spectral region after the edge crest was used to normalize the spectra for atomic absorption.

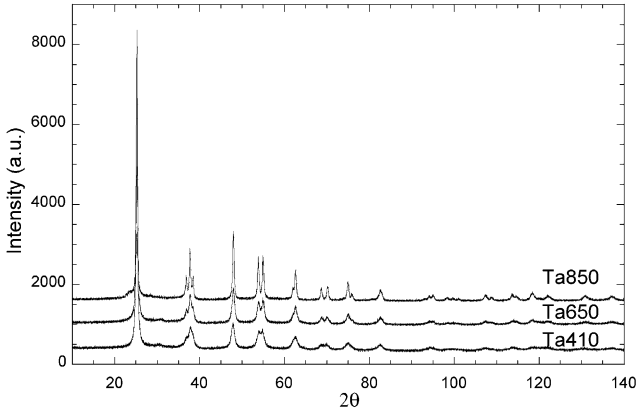


Fig. 2. Measured XRD patterns of Ta-doped anatase samples heated at different temperatures.

## 3. Results and discussion

### 3.1. X-ray diffraction data

X-ray powder diffraction data of doped anatase (Fig. 2), used for XAS measurements, and pure anatase, obtained by the same synthesis method, were Rietveld refined. The refined values of the unit-cell parameters and metal–oxygen bond distances are reported in Table 1. The weak peak at $2\theta \cong 30.3°$ cannot be attributed to the anatase phase and is assigned to the 2 1 1 reflection of brookite (Fig. 3). The wide diffraction peaks due to the small dimensions of the diffracting crystals makes it difficult to precisely determine the unit-cell parameters and metal–oxygen distances. The values reported in Table 1 show a lengthening of the metal–oxygen apical distances of doped anatase at increasing firing temperatures.

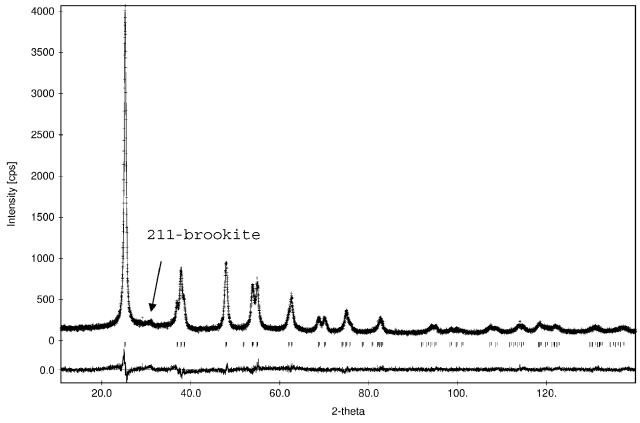


Fig. 3. Observed (crosses), calculated (solid line) and difference (bottom line) plots for the Rietveld refinement of Ta650 sample. The arrow indicates the 211 reflection of brookite, all other reflections refer to anatase phase.

Table 1
Unit-cell parameters, metal-oxygen distances of pure titania samples (Ti410, Ti650), Ta-doped and Nb-doped anatase obtained by rietveld refinements

| Sample | *a* (Å) | *c* (Å) | *d*(Me–O) [×4] (Å) | *d*(Me–O) [×2] (Å) | [a]$R-P$ | [a]$R-B$ |
|---|---|---|---|---|---|---|
| Ti410 | 3.787(1) | 9.498(1) | 1.934(1) | 1.981(2) | 8.17 | 4.03 |
| Ti650 | 3.785(1) | 9.512(1) | 1.934(1) | 1.980(1) | 9.07 | 3.03 |
| Ta410 | 3.802(1) | 9.509(1) | 1.942(1) | 1.981(3) | 6.77 | 6.11 |
| Ta650 | 3.796(1) | 9.518(1) | 1.938(1) | 1.988(3) | 8.07 | 6.15 |
| Ta850 | 3.793(1) | 9.524(2) | 1.935(1) | 1.994(2) | 8.81 | 7.72 |
| Nb10 | 3.796(1) | 9.508(1) | 1.938(1) | 1.986(2) | 8.19 | 4.24 |
| Nb5 | 3.793(1) | 9.505(1) | 1.938(1) | 1.977(2) | 7.53 | 3.31 |

[a] $R-P = 100\frac{\sum|y_{oi}-y_{ci}|}{\sum|y_{oi}|}$; $R-B = 100\frac{\sum|I_o-I_c|}{\sum I_o}$,

$y_{oi}$ = observed intensity at the *i*th step; $y_{ci}$ = calculated intensity at the *i*th step; $I$ = Bragg intensities.

### 3.2. EXAFS data

The EXAFS data were analyzed using the UWXAFS package and theoretical phase functions and amplitudes from FEFF8 [12]. The reliability of the theoretical phases and amplitudes were assessed by applying them to the standard compounds $KTaO_3$ and NbO with known structures. For both Ta- and Nb-doped titania samples, the simulated EXAFS signals were calculated on the basis of the anatase reference structure, supposing the Ta or Nb atoms in the octahedral sites of the anatase structure. According to this structural model, the main contributions to the EXAFS signal consist of two single-scattering paths relative to oxygen shells ($X$–$O_1$ [$\times 4$], $X$–$O_2$ [$\times 2$]) and two single-scattering paths relative to titanium shells ($X$–$Ti_1$ [$\times 4$], $X$–$Ti_2$ [$\times 4$]).

To determine the structural parameters relative to the Ta site, a multiple-shell fit in $R$ space was performed. The FEFFIT routine was used, and data analysis was performed in the ranges $k_{min} = 2.5$ to $k_{max} = 12.6\,Å^{-1}$ and $R_{min} = 1.1$ to $R_{max} = 3.1\,Å$, using a $k$-weight equal to 1. We analyzed the first two coordination shells (consisting of 4 oxygens at a shorter distance and two oxygen atoms at a slightly longer distance), and the third coordination shell (of 4 titanium atoms). The fitting parameters were the Debye–Waller factor ($\sigma^2$), the coordination distances of the first two oxygen shells, and that of the first titanium shell. The coordination numbers of the oxygen shells ($N_1 = 4$, $N_2 = 2$) and the titanium shell ($N_3 = 4$) were kept fixed, as required by the anatase structure. In all cases, a value of the many-body amplitude reduction factor $S_0^2$ equal to 0.7, as obtained from the fit of the reference sample spectra, was used.

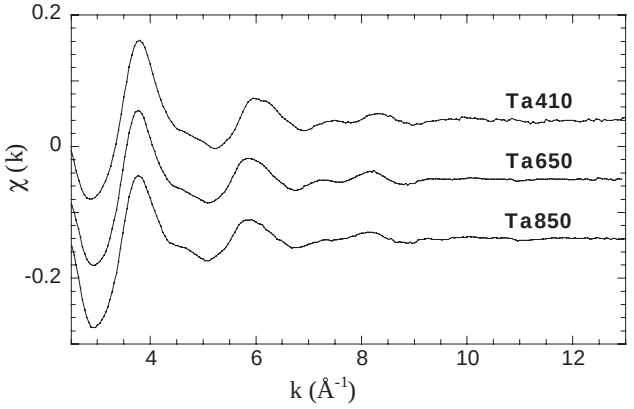


Fig. 4. Experimental raw EXAFS signals of tantalum-doped samples.

In order to determine the structural parameters relative to the Nb site, a multiple-shell fit was performed in the ranges $k_{min} = 3.0$ to $k_{max} = 13.7\,Å^{-1}$ and $R_{min} = 1.0$ to $R_{max} = 3.7\,Å$, with a $k$-weight equal to 1. During the fitting procedure the coordination numbers of the oxygen shells ($N_1 = 4$, $N_2 = 2$) and titanium shells ($N_3 = 4$, $N_4 = 4$) were kept fixed. Due to the poorer quality of the measured spectra of the Nb $K$-edge, it was not possible to separately distinguish the contribution of the first titanium shell from that of the second titanium shell ($X$–$Ti_2$ [$\times 4$]), as required by anatase structure. In order to obtain a satisfactory multiple-shell fit it was necessary to include the contribution of the first two titanium shells. The fitting parameters were the Debye–Waller factor, the coordination distances of the first two oxygen shells, and those of the first two titanium shells; multiple-scattering contributions were not considered. A value of the many-body amplitude reduction factor $S_0^2$ equal to 0.76 was used (determined by the fitting of the reference sample). For all fits, the calculated statistical errors on bond distances were smaller than the uncertainty (0.01 Å) attributed to the EXAFS technique.

#### 3.2.1. Ta-doped samples

The EXAFS spectra (shown in Fig. 4) relative to the Ta-doped titania samples heated at temperatures between 410°C and 850°C do not present remarkable differences, indicating that no important structural modifications occurred upon thermal treatment.

Table 2
Results of EXAFS analysis. Coordination numbers of the different shells were kept fixed to the crystallographic values of anatase

| Sample | $R$-factor[a] | Ta–$O_1$ | | | Ta–$O_2$ | | | Ta–Ti | | |
|---|---|---|---|---|---|---|---|---|---|---|
| | | $r$ (Å) | $N$ | $\sigma^2$ (Å$^2$) | r (Å) | $N$ | $\sigma^2$ (Å$^2$) | $r$ (Å) | $N$ | $\sigma^2$ (Å$^2$) |
| Ta410 | 0.012 | 1.94(1) | 4 | 0.0011(9) | 2.05(2) | 2 | 0.0026(19) | 3.13(4) | 4 | 0.0052(12) |
| Ta650 | 0.007 | 1.95(1) | 4 | 0.0013(11) | 2.08(1) | 2 | 0.0056(24) | 3.14(2) | 4 | 0.0048(7) |
| Ta850 | 0.010 | 1.96(1) | 4 | 0.0010(9) | 2.11(1) | 2 | 0.0065(42) | 3.16(1) | 4 | 0.0081(13) |

[a] $$R\text{-factor} = \frac{\sum_{i=1}^{N}\left\{[\mathrm{Re}(f_i)]^2 + [\mathrm{Im}(f_i)]^2\right\}}{\sum_{i=1}^{N}\left\{[\mathrm{Re}(\tilde{\chi}_{\mathrm{data}_i})]^2 + [\mathrm{Im}(\tilde{\chi}_{\mathrm{data}_i})]^2\right\}},$$

Re = real part; Im = imaginary part; $f_i$=function to minimize.

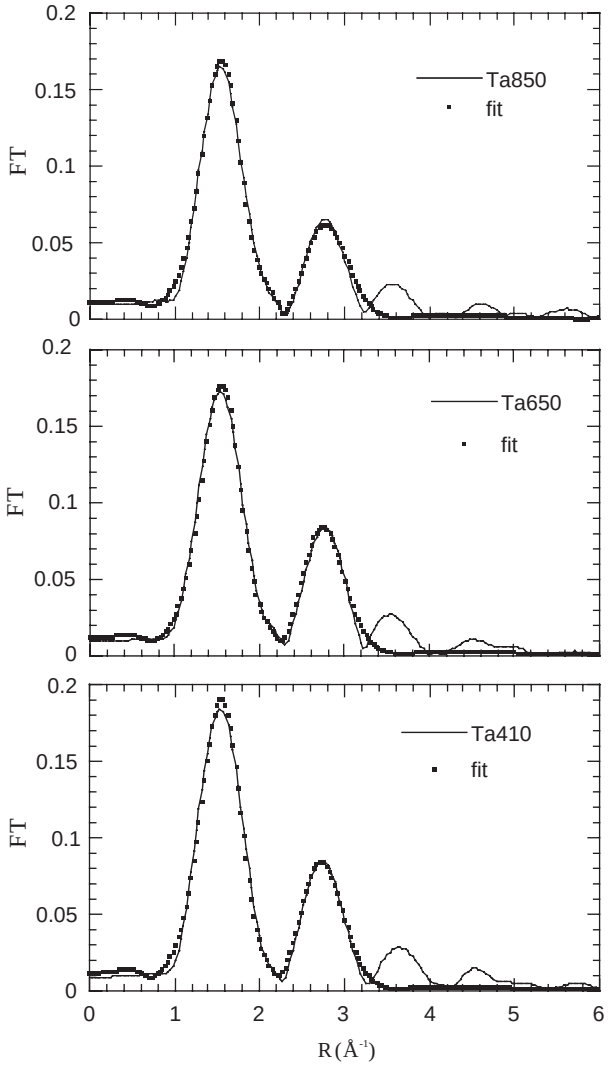


Fig. 5. Fit (dotted lines) to FT of Ta-doped anatase data (solid lines). The fit was obtained in the range $R_{min} = 1.2$ to $R_{max} = 3.1$ Å.

The EXAFS signal was quantitatively analyzed using a fitting procedure on the basis of the anatase structural model. The two oxygen shells strongly overlap in the first peak of the Fourier transform (FT). The second peak (at $R = 2.7$ Å) of the FT corresponds to the third coordination shell. The results of the EXAFS analysis relative to the first two peaks of the FT are reported in Table 2 and shown in Fig. 5. The two obtained oxygen bond distances are noticeably longer than the Ti–O distances expected from the crystallographic model (in pure anatase Ti–O distances are 1.94 and 1.98 Å and Ti–Ti 3.04 Å); nevertheless, the octahedron centered by Ta is distorted, maintaining its tetragonal form. This deformation can be partly explained by considering the different ionic radii of the involved elements (Ta(V) = 0.78 Å; Ti(IV) = 0.74 Å, from Ref. [13]).

A slight, progressive increase in the Ta–O distances and Debye–Waller factors in the samples treated at higher temperatures (650°C and 850°C) can also be noted.

In any case the structural features of all samples, in terms of peak positions and shapes of the FT, remain unchanged, indicating that no incipient anatase–rutile transformation occurred up to 850°C. The EXAFS quantitative analysis indicates that Ta dopant atoms enter the anatase structure, substituting Ti atoms in the octahedral crystallographic site, and that a distortion of the octahedral site occurs as a consequence of this substitution. The good quality of the fit (up to the third coordination shell) demonstrates the correctness of the initial assumption, i.e., that Ta dopant atoms substitute Ti in anatase structure. The hypothesized presence of Ta atoms in possible residual amorphous tantalum oxide/hydroxides was therefore discarded. Indeed, tantalum oxides present quite complicated structures, with Ta–O coordination distances ranging from 1.8 to 2.7 Å [14]. Moreover, we obtained a satisfactory fit of the third coordination shell using a Ta–Ti contribution: in a tantalum oxide structure a Ta–Ta contribution would be expected. In fact, any attempt at fitting the second peak of the observed FT with a Ta–Ta contribution was unsuccessful.

### 3.2.2. *Nb-doped samples*

As regards the Nb-doped titania, only the samples heated up to 410°C (Nb5 and Nb10) were measured. Fig. 6 shows the EXAFS raw data of Nb *K*-edge spectra. As in the case of the Ta samples, quantitative EXAFS analysis was performed on the basis of the anatase structure using two oxygen coordination shells around Nb (consisting of 4 oxygen atoms and 2 oxygen atoms at two slightly different distances) and two titanium coordination shells (both consisting of 4 Ti atoms at different distances). The FT of Nb EXAFS signals of the samples Nb5 and Nb10 and the obtained fits are reported in Fig. 7. It was not possible to fit the first titanium shell without including the contribution of the second titanium shell. As said previously, the poorer

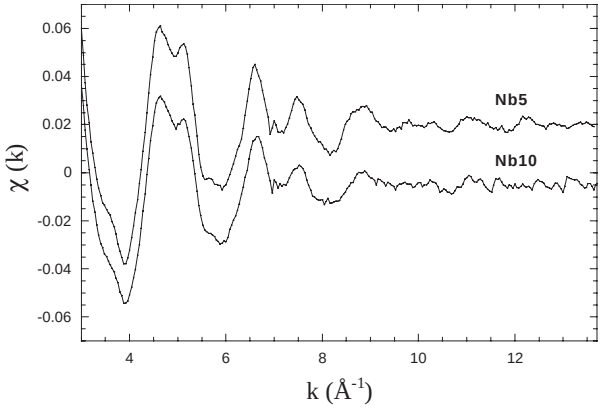


Fig. 6. Experimental raw EXAFS signals of niobium-doped samples.

quality of the measured Nb *K*-edge spectra does not allow to separately resolve the contributions of the first two titanium shells. Table 3 reports the results of the Nb EXAFS analysis. The obtained values are consistent with the results of the Ta EXAFS analysis. Using the same considerations made for the Ta samples, we can thus conclude that the Nb atoms substitute Ti atoms in an anatase structure. Also in this case, in fact, any attempt to fit the second coordination shell with even small amounts of Nb atoms led to a worsening of the fit quality. The FT of samples Nb5 and Nb10 show some differences in the intensity and shape of the second and third peak, anyway the quality of the data does not allow to obtain quantitatively reliable information about this differences.

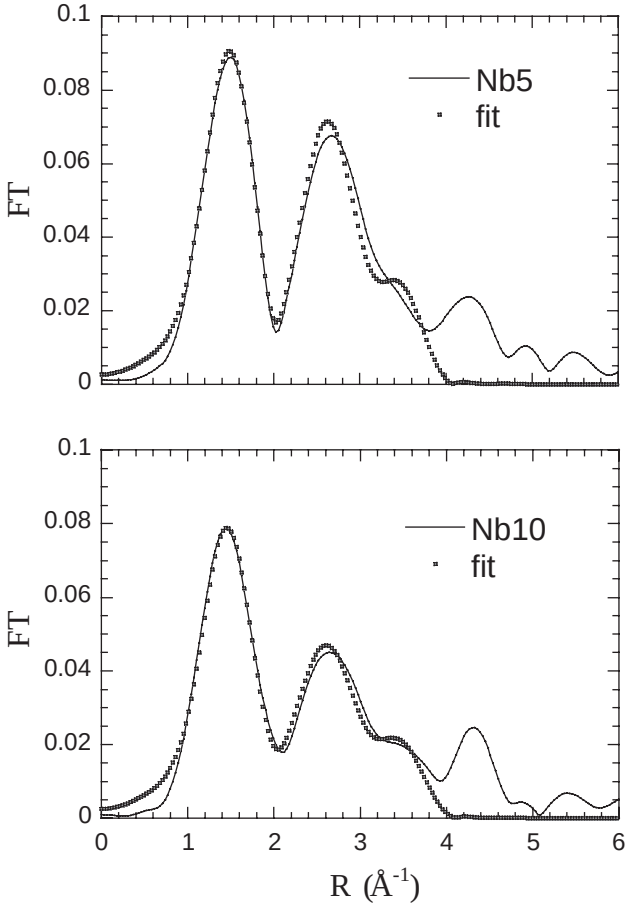


Fig. 7. Fit (dotted lines) to FT of Nb-doped anatase data (solid lines).

### 3.3. XANES data

#### 3.3.1. Ta-doped samples

Fig. 8 shows the normalized $L_I$-edge XANES spectra of the Ta-doped samples and the reference compounds Ta foil, $KTaO_3$ and $Ta_2O_5$. The zero of energy is considered to be the first inflection point in the derivative spectrum of the metallic tantalum at 11,682 eV. The XANES spectra of the samples show strong similarities, indicating the analogy of the Ta site in the three samples. The reference compound $KTaO_3$ has a perovskite-like structure (space group *Pm*-3*m*) in which $Ta^{5+}$ ions are 6-fold coordinated to oxygen atoms in regular octahedral configuration. The real structure of $Ta_2O_5$ is quite complicated, and the metal atoms are expected to be localized at the center of distorted oxygen octahedra or pentagonal bipyramidal polyhedra [15]. In any case, $Ta^{+5}$ ions are localized in low-symmetry coordination sites. The spectra of Fig. 8 show that the $L_I$-edge XANES in the Ta-doped samples exhibit an intense shoulder peak at the low-energy side of the rising edge. In the case of $Ta_2O_5$ this shoulder is less pronounced, and is absent in the $KTaO_3$ reference compound. According to Tanaka et al. [16] this shoulder is attributed to the $2s-5d$ electron transition, and the presence of an intense shoulder in $Ta_2O_5$ spectra

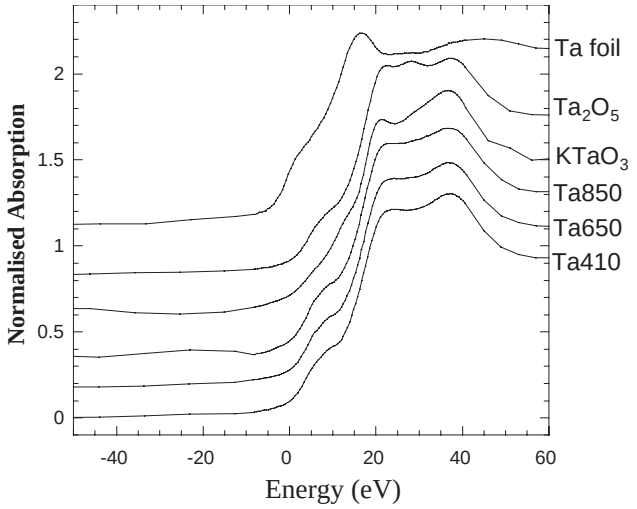


Fig. 8. Normalized $L_I$-edge XANES spectra of Ta-doped samples and reference compounds; the zero of energy is assumed to be at 11,682 eV.

Table 3
Results of Nb EXAFS analysis. Coordination numbers of the different shells were kept fixed to the crystallographic values of anatase

| Sample | Nb–$O_1$ | | | Nb–$O_2$ | | | Nb–Ti | | | Nb–Ti | | |
|---|---|---|---|---|---|---|---|---|---|---|---|---|
| | $r$ (Å) | $N$ | $\sigma^2$ (Å$^2$) | $r$ (Å) | $N$ | $\sigma^2$ (Å$^2$) | $r$ (Å) | $N$ | $\sigma^2$ (Å$^2$) | $r$ (Å) | $N$ | $\sigma^2$ (Å$^2$) |
| Nb5 | 1.95(1) | 4 | 0.0031(11) | 2.07(1) | 2 | 0.0019(19) | 3.13(1) | 4 | 0.0035(3) | 3.95(1) | 4 | 0.0052(9) |
| Nb10 | 1.94(1) | 4 | 0.0024(3) | 2.08(1) | 2 | 0.0012(8) | 3.12(1) | 4 | 0.0068(4) | 3.96(1) | 4 | 0.0077(11) |

*R*-factor for Nb5 = 0.008; *R*-factor for Nb10 = 0.010.

indicates that tantalum ions are located at a center of distorted symmetry. In $KTaO_3$ the Ta atoms are located at the center of a regular octahedral site, and in the XANES spectra this shoulder is absent. The analogy between the low-energy side shoulder of $Ta_2O_5$ and Ta-doped samples XANES spectra suggests that, in our samples, the Ta atoms are located in distorted octahedral sites, as also indicated by the EXAFS quantitative analysis. Regarding the energy position of the absorption thresholds, the first peak in the derivative spectrum of titania and $Ta_2O_5$ XANES spectra is shifted by +5 eV with respect to the absorption threshold of tantalum metal. The positive shift of the threshold by 5 eV in both titania and $Ta_2O_5$ spectra (Ta-foil main-edge position = 11,691 eV; Ta-doped samples main-edge position = 11,696 eV) indicates that, in all our samples, the formal valence of tantalum is +5, as in the reference tantalum oxide. According to our XAFS results, Ta ions with +5 formal valence enter the anatase structure, occupying distorted octahedral sites.

### 3.3.2. *Nb-doped samples*

The normalized *K*-edge spectra of Nb5 and Nb10 samples and the reference compounds Nb foil, $NbO_2$, $NaNbO_3$ and $Nb_2O_5$ are reported in Fig. 9. The zero of energy is taken to be the first inflection point of the niobium metal in the derivative spectrum at 18,986 eV. The XANES spectra of titania samples doped with different amounts of Nb (respectively, 5% and 10%) are almost identical. They are characterized by a weak pre-edge absorption shoulder which is due to $1s-4d$ electronic transition [17]. This weak pre-edge absorption shoulder is also visible in the XANES spectra of reference compound $Nb_2O_5$, while it is not present in the spectra of reference compounds $NaNbO_3$ and $NbO_2$. Even if the crystal structure of $Nb_2O_5$ is quite complicated, the Nb atoms are nevertheless expected to be localized at the center of distorted oxygen polyhedra. The crystal structure of reference compound

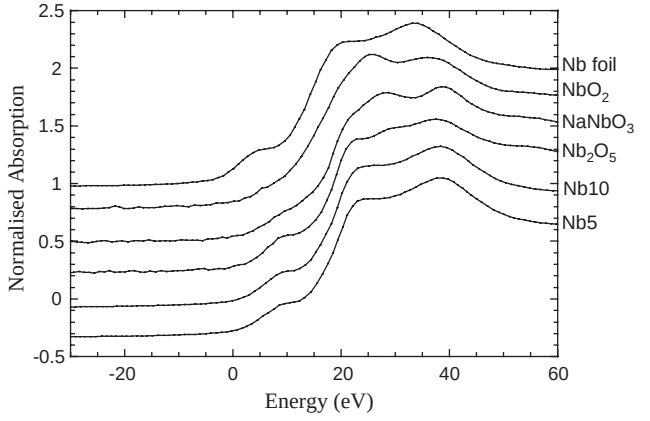


Fig. 9. Normalized *K*-edge XANES spectra of Nb-doped samples and reference compounds; the zero of energy is assumed to be at 18,986 eV.

$NbO_2$ can be described as chains of $NbO_6$ edge-sharing octahedra cross linked by corner sharing, and the Nb–O distances of the octahedra lay between 1.92 and 2.23 Å [18]. Sodium niobate, $NaNbO_3$, is characterized by a perovskite-like structure where the niobium atoms are 6-fold coordinated to oxygens in regular octahedral configuration [19]. The pre-edge absorption shoulder can be reasonably associated to the presence of a distorted coordination environment of the Nb atoms. The analogy between the absorption shoulder of $Nb_2O_5$ and Nb-doped titania XANES spectra suggests that, in our samples, the Nb atoms are located in distorted octahedral sites, as also indicated by EXAFS analysis, and as previously observed for the Ta atoms in Ta-doped samples. The derivative maximum of the Nb-doped samples and of the reference compound $Nb_2O_5$ (main-edge position = 19,019 eV) is 5 eV shifted towards higher energy with respect to the position of the absorption threshold of Nb-foil (main-edge position = 19,014 eV), indicating that Nb ions are dispersed in the titania matrix with oxidation state +5.

## 4. Conclusions

The data analysis results reported in the previous sections indicate that, in nanostructured anatase, both niobium and tantalum atoms present in low concentration (10% for Ta, 5% and 10% for Nb) are completely dispersed in solid solution. There was no evidence to suggest the presence of Ta or Nb metallic clusters. In quantitative EXAFS analysis we considered the Ta or Nb second coordination shell as composed solely of Ti atoms. No Ta or Nb atoms were observed in second coordination shell, suggesting that Ta and Nb ions do not interact with each other. At these low dopant concentrations, Ta and Nb ions are randomly dispersed in the crystallographic sites of anatase structure.

Our results are consistent with the conclusions derived by Arbiol et al. [20] in their study on Nb-doped $TiO_2$ samples synthesized by induced laser pyrolisis. An X-ray Photoelectron Spectroscopy (XPS) study of Nb-doped $TiO_2$ thin films [21] confirm that the oxidation state of niobium is +5.

XANES spectra, in comparison with the standard compounds with known Ta or Nb valence state, show that the oxidation state of dopant tantalum and niobium in titania (anatase) is +5. In order to maintain the equilibrium of charges, the extrapositive charge due to $Nb^{5+}$ or $Ta^{5+}$ may be compensated by the creation of an equivalent amount of $Ti^{3+}$ ions [22], or by the presence of vacancies in the cation sites. As the results of quantitative EXAFS analysis indicate that dopant Ta and Nb atoms are dispersed in crystallographic sites of the anatase structure, and that no segregation of these metals was found, we believe that the cause of the

hindered coarsening of doped $TiO_2$ is related to low ionic mobility within the particles.

## References


[1] D.D. Beck, R.W. Siegel, J. Mater. Res. 7 (1992) 2840–2845.
[2] G. Sberveglieri, L.E. Depero, M. Ferroni, V. Guidi, G. Martinelli, P. Nelli, C. Perego, L. Sangaletti, Adv. Mater. 8 (1996) 334–337.
[3] M.C. Carotta, M. Ferroni, V. Guidi, G. Martinelli, Adv. Mater. 11 (1999) 943–946.
[4] E. Traversa, M.L. Di Vona, S. Licoccia, M. Sacerdoti, M.C. Carotta, L. Crema, G. Martinelli, J. Sol–Gel Sci. Technol. 22 (2001) 167–179.
[5] H. Zhang, J.F. Banfield, Am. Mineral. 84 (1999) 528–535.
[6] B. O'Regan, M. Grätzel, Nature 353 (1991) 737.
[7] B. Poumellec, F. Lagnel, J.F. Marucco, B. Touzelin, Phys. Stat. Sol. (b) 133 (1986) 371.
[8] F. Picard-Lagnel, B. Poumellec, R. Cortes, J. Phys. Chem. Solids 50 (1989) 1211.
[9] D.C. Hague, M.J. Mayo, J. Am. Ceram. Soc. 77 (1994) 1957.
[10] R.A. Young, J. Appl. Crystallogr. 28 (1995) 366–367.
[11] S. Pascarelli, F. Boscherini, F. D'Acapito, J. Hrdy, C. Meneghini, S. Mobilio, J. Synchrotron Radiat. 3 (1996) 147–155.
[12] A.L. Ankudinov, B. Ravel, J.J. Rehr, S.D. Conradson, Phys. Rev. B 58 (1998) 7565–7576.
[13] R.D. Shannon, Acta Crystallogr. A 32 (1976) 751–767.
[14] H.U. Hummel, R. Fackler, P. Remmert, Chem. Ber. 125 (1992) 551–556.
[15] N.C. Stephenson, R.S. Roth, Acta Crystallogr. B 27 (1971) 1037–1044.
[16] T. Tanaka, H. Nojima, T. Yamamoto, S. Takenaka, T. Funabiki, S. Yoshida, Phys. Chem. Chem. Phys. 1 (1999) 5235–5239.
[17] M. Antonio, I. Song, H. Yamada, J. Solid State Chem. 93 (1991) 183–192.
[18] A.K. Cheetham, C.N. Rao, Acta Crystallogr. B 32 (1976) 1579–1580.
[19] A.C. Sakowski-Cowley, K. Lukaszewicz, H.D. Megaw, Acta Crystallogr. B 25 (1969) 851–865.
[20] J. Arbiol, J. Cerdà, G. Dezanneau, A. Cirera, F. Peiró, A. Cornet, J.R. Morante, J. Appl. Phys. 92 (2002) 853–861.
[21] M.Z. Atashbar, H.T. Sun, B. Gong, W. Wlodarski, R. Lamb, Thin Solid Films 326 (1998) 238.
[22] M. Valigi, D. Cordischi, G. Minelli, P. Natale, P. Keijzers, J. Solid State Chem. 77 (1988) 255.